INSTITUTE OF PHYSICS PUBLISHING PHYSIOLOGICAL MEASUREMENT

Physiol. Meas. **22** (2001) 9–18 www.iop.org/Journals/pm PII: S0967-3334(01)19980-6

A 3D electrical impedance tomography (EIT) system for breast cancer detection

V Cherepenin[1], A Karpov[2], A Korjenevsky[1], V Kornienko[1], A Mazaletskaya[3], D Mazourov[4] and D Meister[5]

[1] Institute of Radio-Engineering and Electronics of Russian Academy of Sciences, Moscow, Russia
[2] Clinical Hospital No 9, Yaroslavl, Russia
[3] Yaroslavl State University, Russia
[4] Regional Oncological Hospital, Yaroslavl, Russia
[5] Technology Commercialization International, Inc., Albuquerque, NM, USA

E-mail: korjenevsky@cplire.ru, almaz@yars.free.net and tcintl@nm.net

Received 12 December 2000

Abstract

A medical device which allows imaging of the distribution of conductivity in 3D in regions below the skin surface has been developed and tested. Its purpose is to enable early detection and preliminary diagnosis of breast tumours. Design of the measuring system and software are described. Results of clinical evaluation of the system are presented. EIT images of healthy and cancerous breasts are presented and discussed. The system is able to visualize various states of the breast and it may be possible to apply it to breast cancer detection.

Keywords: electrical impedance tomography, breast cancer detection, bio-impedance, medical imaging

1. Introduction

The electrical conductivity of many tumours, in particular the malignant tumours of the breast, may significantly differ from the conductivity of surrounding normal tissue (Rigaud *et al* 1996). This provides a possible way to provide an efficient, safe and inexpensive method to detect and localize such tumours, using electrical impedance tomography (EIT). This technique enables visualization of the spatial distribution of conductivity in the human body; several research groups work on EIT systems for breast imaging (see, for example, Tunstall *et al* 1998, Wtorek *et al* 1999). Application of this method to breast cancer detection requires special design of the measuring system and image reconstruction algorithm, as imaging of a three-dimensional distribution of conductivity is required. The resolution of the EIT system falls significantly with increasing distance from measuring electrodes, and traditional EIT measurement schemes are unsuitable for mammography because of this. A large number of electrodes, which are required to provide acceptable resolution of the system, leads to enormous increases in computation time for image reconstruction.

The prototype of the breast cancer detection device (BCDD), presented in this paper, which is suitable for carrying out clinical recordings, has been developed in the Institute of the Radio-Engineering and Electronics of the Russian Academy of Sciences with the support of Technology Commercialization International, Inc. (USA). It is a 3D EIT system which consists of a compact array of electrodes positioned over the tissue being measured, two additional electrodes placed remotely from the array of electrodes, a source of alternating (AC) current, a means to measure potential difference and computing means to reconstruct and visualize the conductivity distribution as stack of tomographic images.

A comparative analysis of electrical impedance images obtained with the new system in normal and cancerous breasts is presented in this paper.

2. Materials and methods

2.1. Measuring system

The measurements are carried out using 256 electrodes, which are arranged in a square matrix with sides of 12 cm. The electrodes are supported on a rigid plane, from which each electrode protrudes. During an examination, the plane of electrodes is pressed against the breast, so flattening it toward the chest. This increases the number of electrodes in contact with the breast and decreases the thickness of the tissue layer to be measured. The 3D EIT system includes an output multiplexer, which is connected to the electrode array and is the means by which an alternating current (AC) source is connected to one of the electrodes in the array. An input multiplexer connects one of the remaining electrodes of the array to a potential difference measuring unit. A microprocessor in the 3D EIT system and computer determine through which electrode current is driven and which electrode is selected for potential difference measurement. Two single remote electrodes are attached to the extremities of the patient. One remote electrode is connected directly to a safe AC source (0.2 mA, at 10 kHz, whereas the maximum allowable safe level is 1.0 mA, at 10 kHz). The other remote electrode is connected directly to the potential difference detector. The 3D EIT system operation is controlled by a microprocessor and computer.

The output multiplexer switches a single lead from the AC source to activate a single electrode in the electrode array at a time, instead of activating pairs of electrodes. The second activated electrode is a remote electrode that is always on. The input multiplexer functions in a similar fashion. The potential difference detector measures the difference between the selected array electrode and a remote rest electrode. For a given input electrode, the output multiplexer sequences through all the other electrodes in the array while the potential difference detector makes its measurements. Then the input electrode is switched and the output multiplexer sequence repeated. Switching a single lead at a time reduces the spurious couplings which arise from cross-talk in the multiplexer. It also simplifies the device and reduces its cost. The distance of the remote electrodes from the electrode array supports the assumption that the unperturbed equipotential surfaces of electric field are spherical in the examination area. It simplifies and speeds up the conductivity reconstruction calculations.

The current injection and voltage measurement circuitry is similar to the one in our electrical impedance tomograph for static imaging (Cherepenin *et al* 1995, Korjenevsky *et al* 1997). In the current source, a digital-to-analogue converter provides the input signal for a voltage-to-current converter which consists of three operational amplifiers. In the potential-difference-measuring unit, an analogue synchronous detector and switchable integrator convert input AC potential differences to DC before analogue-to-digital conversion. A synchronous detector provides measurement of the real part of impedance. A 16-bit analogue-to-digital

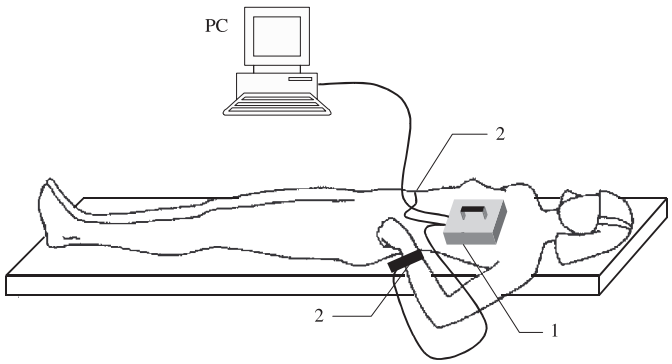

Figure 1. Physical configuration of the system and measuring procedure: 1—plane with 256 electrodes, 2—remote electrodes.

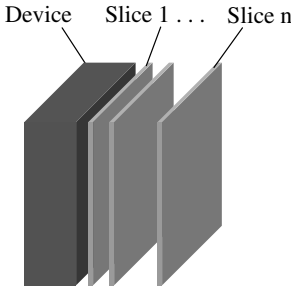

Figure 2. 3D imaging planes.

converter measures voltage. A fast-response circuit for DC potential compensation enables reliable measurements with the stainless steel electrodes that are used. A full measurement cycle (65 280 voltage measurements) takes less than 20 s. Since some of the electrodes on the planar electrode array can be out of contact with patient's body, the measuring system is provided with a voltage threshold detector. This is connected to the current source and checks the quality of contacts. Information from this circuit is used during image reconstruction. Figure 1 illustrates the physical configuration of the system and measurement procedure.

2.2. Reconstruction software

The method of back-projection is one of the fastest in electrical impedance tomography and seems most suitable for 3D applications like this one; for 256 electrodes, the time required for calculations is critical. Our EIT system uses a method of weighted back projection along equipotential surfaces of the electric field to reconstruct the 3D conductivity distribution. It provides visualization of several tomographic cross-sections ('slices'), which are parallel to the electrode array (figure 2).

It is assumed that where the electric current is injected through one of the electrodes in a planar array and the remote common electrode, equipotential surfaces near the array are spherical. The procedure of back projection is reduced to the following. For some point with co-ordinates (x, y, z) inside the object being imaged, the distance is determined between this point and the injecting electrode of the array. This is equal to the radius r of the equipotential

surface containing the point where the conductivity is reconstructed. Knowing this radius, it is possible to determine the line of intersection of the equipotential surface with the surface on which the electrodes are arranged. When the electrodes are arranged on the plane, given by equation $z = 0$, this line is the circle lying in the (x, y) plane having its centre at the point where the injecting electrode is located, and having radius r. Conductivity S (in arbitrary units) at the chosen point is calculated according to the equation

$$S(x, y, z) = 1 + W_1(z) \sum_i \left(\int_{L(x,y,z,i)} W_2(l)\, \mathrm{d}l \right)^{-1} \int_{L(x,y,z,i)} W_2(l)(E_r(l) - E_m(l))/E_r(l)\, \mathrm{d}l$$

where i is the number of the injecting electrode, and $L(x, y, z, i)$ is the line of intersection of the equipotential surface with the surface on which the electrodes are arranged (a circle with radius r). The components of the electric field vector $\vec{E}_m$ are first calculated at the nodes of the grid between the electrodes as the potential differences between adjacent electrodes in the x and y directions. Then these components are linearly interpolated to the current point of integration on the line L and the magnitude of this vector E_m is calculated. The reference intensity of the electric field E_r corresponds to a homogeneous medium and is calculated numerically using the reference data set synthesis technique (Korjenevsky 1995) to improve static imaging. A weighting coefficient $W_1(z)$ corrects the decrease of sensitivity with depth as $W_1 = (z + \alpha)/(z + \beta)$, $\alpha \ll \beta$.

The weighting coefficient W_2 provides a relatively greater contribution to the calculated conductivity of those points on line L, which are located closer to the point at which the conductivity is reconstructed. The 3D EIT system uses the equation $W_2 = 1/R^4 = 1/\left((x - x_l)^2 + (y - y_l)^2 + z^2\right)^2$, where R is the distance between the point where the conductivity is reconstructed and the current point on the line along which integration is being carried out; the index l refers to the coordinates of this point.

Whenever it is difficult to produce sufficient contact of all the electrodes with the patient's body, then the output voltage of the threshold detector is used to determine whether the electrode being used at any particular moment has sufficient contact with the body. The values of the potential differences measured from electrodes that have insufficient body contact cannot be used properly in the process of conductivity reconstruction. Instead, values of potential differences calculated based on a homogeneous conductivity distribution are used.

The resulting electrical impedance image represents tissue conductivity along a grey scale from dark to light, which represents low to high conductivity. The time that is required for the reconstruction of conductivity in seven cross-sectional slices (each with a 8 mm depth step) is less than 1 min with a Pentium II 300 MHz processor.

2.3. Testing of the system in a saline filled tank and the male breast

The device was tested on a saline filled tank and on the male volunteers (the male breast, which is not as complicated as the female breast, was investigated in the first trials). The tank measurements were carried out with the device placed horizontally above the open surface of the saline. The tank, filled with 1% sodium chloride solution, was 10 cm deep and 30×30 cm^2 square. The remote electrodes were placed on the corners at the bottom of the tank. Testing in the tank has demonstrated the accuracy of imaging with test objects up to 5 cm from the planar electrode array (figure 3). A hollow glass cylinder, 5 cm in diameter and 9 cm high (wall thickness 0.5 cm) was immersed vertically in the saline. The distance between the electrodes and top of the test cylinder was approximately 1 cm. In the images, it may be seen that the cylinder appears as a circle at any depth. The structure of the test object appears to simplify

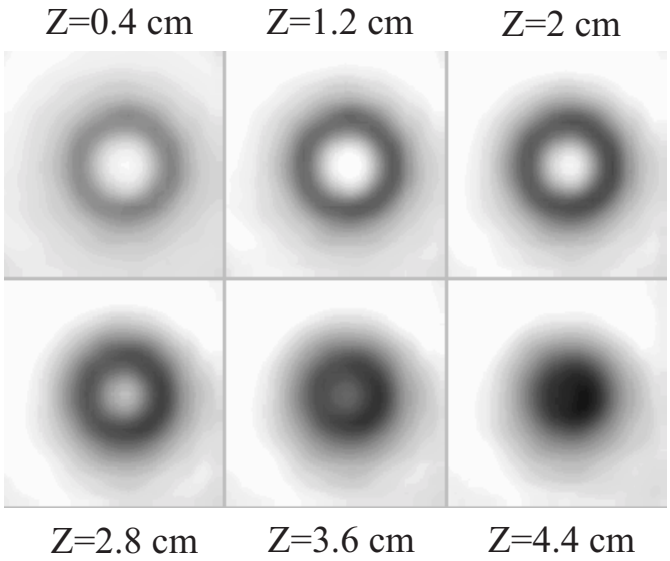

Figure 3. Imaging of a glass cylinder immersed vertically into the saline filled tank.

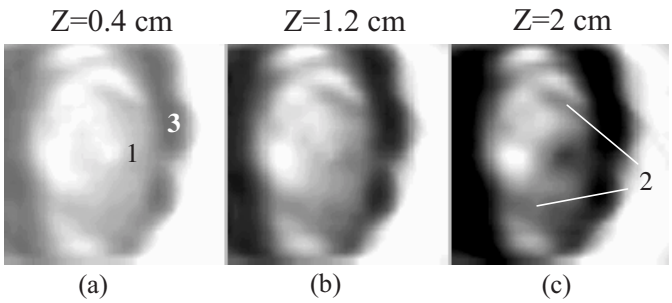

Figure 4. Male breast images at different cross-sections: (a) 0.4 cm, (b) 1.2 cm, (c) 2 cm from the skin surface. Presumed anatomical correlations: 1—nipple, 2—ribs, 3—zone of artefacts, which correspond to the boundary between good and faulty contacts on the electrode plane.

with depth, presumably due to a decrease in device resolution. Other tank measurements were performed with small test objects in order to estimate resolution and sensitivity of the system. In such tests the device clearly imaged an 8 mm ball made from aluminium foil at a depth of 2 cm.

An example of *in vivo* imaging is demonstrated in figure 4. The measurements were made on the breast of a male volunteer, aged 40 years, in good health and of normal body habitus. Many electrodes were in poor contact with the body. The areas of poor contact appear as white fields accompanied with dark artefacts on the periphery of the images. Nevertheless, the central parts of the images, corresponding to three depth levels, appear to demonstrate good correlation with underlying anatomic structures. The nipple area appears to be visible as a highly-conductive area on the most superficial image (figure 4(a)) but has low conductivity in deeper layers (figure 4(b, c)). The ribs become appear to be visible in an image slice 1 cm deep. The muscle tissues appear to be homogeneous in the imaged area.

3. Clinical measurements

21 women with tumours in one breast were examined. The size of tumours, determined by x-ray mammography, was 1.5 to 5 cm. The contralateral breast was assumed to be healthy. Examinations were made in two positions—lying and standing. This resulted in 84 electrical impedance mammograms (EIMs) in total. These were sorted into five groups. (1) 42 EIMs in the normal breast contralateral to that containing the tumour. (2) 42 EIMs in the breast with a clinical diagnosis of breast cancer. Group (2) was subdivided according to whether focal abnormalities could be seen on visual inspection of EIM. (3) 16 EIMs without focal abnormalities. (4) 26 EIMs with such abnormalities. The focal abnormalities in this group were confirmed by x-ray mammography. They appeared on EIT images as white (highly conductive) areas. (5) This group, 13 EIMs, was created by selection of the peak highly conductive areas of group (4). It therefore refers not to whole images, but merely the properties of the most conductive regions in the pathological breasts of patients with cancer. The clinical diagnosis was confirmed by x-ray mammography prior to surgery and histology after surgery and excision of the tumour. The average age of patients was 60 years; 50% of patients had arterial hypertension; 27% had a family history of cancer.

EIM were reconstructed every 8 mm down to a depth of 6 cm (seven scanning planes). Wet gauze was placed between the breast skin and electrode array to improve electric contact. Image acquisition in one patient (preparation, measurements, image reconstruction and processing) took about 15–20 min. The analysis of EIM included (i) visual analysis of images at different depths, (ii) image filtering and calculation of generalized characteristics of conductivity and its variability (average, standard deviation, max and min values) and (iii) presentation of images according to the frequency distribution of conductivity and comparison of the frequency distribution of healthy and ill breast tissues using non-parametric analysis of difference (Kolmogorov–Smirnov criteria).

4. Results

4.1. Breast images

EIM were compared with mammograms obtained from the same scanning plane. With increasing depth, the scanning area of breast decreases, due to limitations in the data. In all images given in this paper, the peripheral area, especially the corners, is the region which has bad contacts, so peripheral dark contours are artefacts which are related to the transition from good to bad contacts. Only the central regions inside these contours are therefore suitable for analysis.

The normal breast image (figure 5) is characterized by an absence of focal abnormalities and has smooth contours of conductivity ('mosaic'). These are seen in scanning planes. Breast cancer EIMs (figure 6) are characterized by focal abnormalities which appear as clear-cut light areas of high conductivity. In the EIM, the focus size varied from 2.0×0.8 cm^2 up to 3.2×3.0 cm^2, spreading to a depth of 3 cm.

4.2. Statistics

During analysis of these EIM images, focal abnormalities in the images, which represent tumours, were seen in 14 of a total of 21 studies, 67%. Another four EIMs without clear abnormalities were nevertheless classified as abnormal due to a conductivity distribution different from the typical distribution in normal breast. As a result, 86% of examinations were

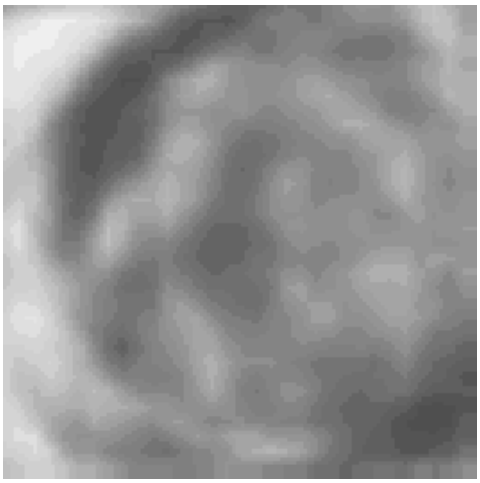

Figure 5. EIM image of intact breast at a depth of 1.2 cm.

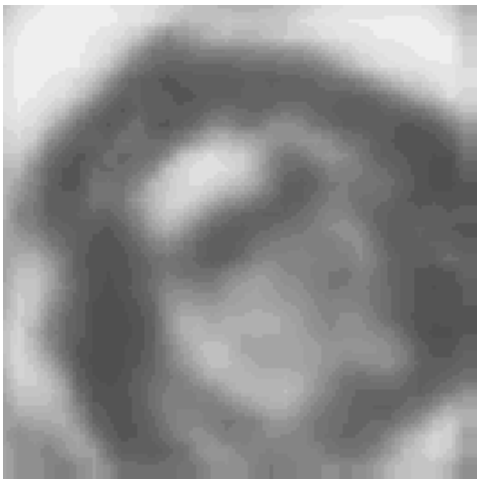

Figure 6. EIM image of breast cancer with a 1.2 cm scanning plane; the cancerous area is above and to the left of the centre of the image.

found to be fully or partially consistent with diagnoses made by other independent methods. The causes of data mismatch included (i) enlarged breasts hamper examination due to limited scanning depth, (ii) some BCDD examinations were performed after medical treatments such as puncture, biopsy, or x-ray therapy), which influenced the EIM.

Tissue conductivity was calculated in conventional units. The average conductivity of intact and ill breasts at all scanning planes had a normal distribution. For example, at the most superficial plane, the mean value was $\mu = 0.89$ with a standard deviation $\delta = 0.034$.

Average breast conductivity and standard deviations for groups (1) and (2) at different scanning planes are given in table 1. A systematic decrease of conductivity with depth is observed and may be attributed to the reconstruction software. It should be possible to improve this in the future by choosing more correct weighting coefficients for the back projection procedure. No statistically significant differences in average conductivity between these groups were found.

Table 1. Average breast conductivity in group (1) and group (2).

	Scanning plane 1 (0.4 cm)	Scanning plane 3 (2.0 cm)	Scanning plane 5 (3.6 cm)
Intact breast	0.89 ± 0.028	0.77 ± 0.056	0.68 ± 0.058
Cancer	0.88 ± 0.042	0.76 ± 0.077	0.69 ± 0.066

Table 2. Average breast conductivity after subdividing of group (2).

	Scanning plane 1 (0.4 cm)	Scanning plane 3 (2.0 cm)	Scanning plane 5 (3.6 cm)
Group 1	0.89 ± 0.028	0.77 ± 0.056	0.68 ± 0.058
Group 3	0.86 ± 0.026	0.72 ± 0.049	0.66 ± 0.053
Group 4	0.91 ± 0.037	0.81 ± 0.066	0.70 ± 0.067
Group 5	0.99 ± 0.038	0.97 ± 0.067	0.96 ± 0.026

Average breast tissue conductivity in groups (3)–(5) is presented in table 2. The averages of groups across scanning planes are significantly different, using variance analysis. With a multiple comparison method—the Newman–Keils criterion (Glantz 1994) we have shown that averages of all groups at scanning planes 1 and 3 significantly differ from each other. At the fifth scanning plane, there was no significant difference.

4.3. Conductivity distribution on EIM

To compare images more accurately, we used histograms of conductivity. To obtain a reference distribution, we built an average histogram of frequency distribution of conductivity for intact breasts (average histogram); it is close to a Gaussian distribution. This was then compared with histograms of each EIM in groups (2), (3) and (4). The histograms were compared qualitatively using such parameters as modality (the number of the local maxima in histograms) and symmetry. In groups (3) and (4), the percentage of multi-modal distributions increased with the increase of scanning depth.

For quantitative estimation of the difference of conductivity distribution between the normal group (1) and the EIMs from groups (3) and (4) (figure 7), we used the concept of the distribution difference value (D_x). The calculation of D_x was carried out through the Kolmogorov–Smirnov algorithm (see, for example, Gubler 1978). According to Gubler, a high significance is observed with distribution difference values of 35–50%. For $D_x = 40\%$, as a criterion of separation of distributions, we found that for group (3) and group (4) 90% of EIM diagrams (19 of 21) have a significant difference from the normal group (1).

5. Discussion

These first experiments have demonstrated that a single frequency static imaging EIT system with 256 electrodes, arranged in a two-dimensional square, is capable of producing images which may be usable in breast cancer detection. The breast is a complex alveolar–tubular gland which consists of 15–20 lobules, encircled by adipose tissue. The complicated anatomical structure of breast tissue may explain the 'mosaic' electrical impedance image of healthy breast. The appearance of focal abnormalities in EIM as clear-cut light areas is due to increases in local conductivity. This has been described for tumours, which are usually vascular. Such focal abnormalities found in 67% of patients with breast cancer.

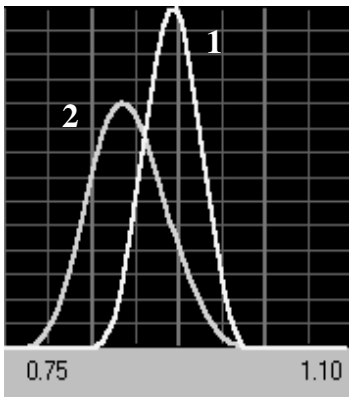

Figure 7. Comparison of EIM histograms: 1—average histogram of normal breast images; 2—one histogram for a breast with cancer; the D_x parameter is 51% for these two distributions.

Analysis of the average conductivity of breast tissues showed that, in groups (1), (3), (4) and (5), it differs significantly at all scanning planes. In the regions estimated solely to correspond to tumour (group (5)) increased conductivity was apparent at all scanning planes. A decrease of average conductivity in breast tissues in group (3) (breasts with tumour but no focal abnormalities on EIM) may be due to changing of electrical characteristics after x-ray medical treatment or a background state preceding the appearance of tumour.

To determine differences in conductivity histograms in groups (1)–(4), it was necessary to use non-parametric criteria. The approach developed in this work for estimating the difference of conductivity histograms, based on the Kolmogorov–Smirnov criterion, may be useable in population screening examinations. Further planned studies will involve a larger number of patients, and will take into account the menstrual cycle, presence of cysts and other benign changes in breast tissue, in order to get more reliable data.

Acknowledgments

This work was supported by Technology Commercialization International, Inc., 1650 University Boulevard, NE, Albuquerque, NM 87102, USA as part of the TC International Breast Cancer Detection Device program.

References

Cherepenin V A, Korjenevsky A V, Kornienko V N, Kultiasov M Y and Kultiasov Y S 1995 The electrical impedance tomograph: new capabilities *Proc. 9th Int. Conf. on Electrical Bio-Impedance (Heidelberg, 1995)* pp 430–33

Glantz S A 1994 *Primer of Biostatistics* (New York: McGraw-Hill)

Gubler E 1978 *Calculation Methods of Analysis and Recognition of Pathological Processes* (Leningrad: Meditsina)

Korjenevsky A V 1995 Reconstruction of absolute conductivity distribution in electrical impedance tomography *Proc. 9th Int. Conf. on Electrical Bio-Impedance (Heidelberg, 1995)* pp 532–5

Korjenevsky A V, Kornienko V N, Kultiasov M Y, Kultiasov Y S and Cherepenin V A 1997 *Prib. Tekh. Exp.* No 3 133-40 (Engl. transl. Korzhenevskii A V, Kornienko V N, Kul'tiasov M Y, Kul'tiasov Y S and Cherepenin V A Electrical impedance computerized tomograph for medical applications *Instrum. Exp. Tech.* **40** 415–21)

Rigaud B, Morucci J P and Chauveau N 1996 Bioelectrical impedance techniques in medicine part I: bioimpedance measurements second section: impedance spectrometry *Crit. Rev. Biomed. Eng.* **24** 257–351

Tunstall B, Wang W, Cheng Z, McCormik M, Walker R and Rew D 1998 *In vitro* study results from De Montfort Mk1 electrical impedance mammography system *Proc. 10th Int. Conf. on Electrical Bio-Impedance (Barcelona, 1998)* pp 525–28

Wtorek J, Stelter J and Nowakowski A 1999 Impedance mammograph 3D phantom studies *Ann. NY Acad. Sci.* **873** 520–33